Actin filaments on myosin beds: The velocity distribution

L. Bourdieu,[1] M. O. Magnasco,[1] D. A. Winkelmann,[2] and A. Libchaber[1,3,*]
[1]*The Rockefeller University, 1230 York Avenue, New York, New York 10021*
[2]*Department of Pathology, Robert Wood Johnson Medical School, Piscataway, New Jersey 08854*
[3]*NEC Research Institute, 4 Independence Way, Princeton, New Jersey 08540*
(Received 6 July 1995)

In vitro studies of actin filaments sliding on a myosin-coated surface are analyzed, filament by filament, at a sampling rate of 30 per second. For each filament, the mean arc length coordinate is computed and histograms of instantaneous velocities, along the arc length, are established. Two types of motion are observed, depending on the experimental conditions. The first one is characterized by a homogeneous flow, with well defined velocities. In this regime, specific defects are a constitutive part of the flow. It is observed at high temperature, at high myosin coverage, and with a particular mode of attachment of myosin to the surface. The second regime shows no clear velocity selection, but a broadband distribution. It is characterized by high friction and is observed at low temperature or low myosin density.

PACS number(s): 87.22.Jb, 42.30.Va

I. INTRODUCTION

Motor proteins are involved in a large variety of important cell functions [1,2]. For the motors to operate, ATP (adenosine triphosphate) is needed, both as an energy source and for its enzymatic activity. In the last ten years, a large number of new molecular motors have been discovered [1]. So called "*in vitro* motility assays" are widely used to characterize their properties [3–7]. In the experiment described in this paper, the motion of actin filaments (usually called F-actin) on a surface coated with myosin motor proteins is observed by video fluorescence microscopy (Fig. 1). The analysis of the filament velocity under different experimental conditions gives information about the physical and thermodynamic properties of the motors. The filament velocity and the kicking force can be measured and the myosin-ATP cycle and its duty ratio, it is hoped, can be deduced by varying the temperature and the myosin surface density.

One difficulty of the motion analysis arises from the enormous information content of video images and thus the complexity of analyzing the velocity distribution. Typically, about ten actin filaments, approximately 1 to 10 μm long, are visualized on a screen of size 80×60 μm^2. To determine a filament velocity, the position either of the leading edge or of the centroid [6] of the filament is usually used. In this paper, we present an intricate program to compute automatically and precisely the velocity of a filament along its trajectory. Each video frame is acquired on a workstation, is thresholded, and is filtered. By superimposing successive frames, each filament is identified in time, its successive positions are obtained, and the skeleton of its trajectory is computed. After the trajectory is calculated, the coordinate of the filament is then deduced in an arc length representation. Thereupon, instantaneous velocities of a large number of filaments on their tracks can be computed and their velocity distribution established. We use this program to

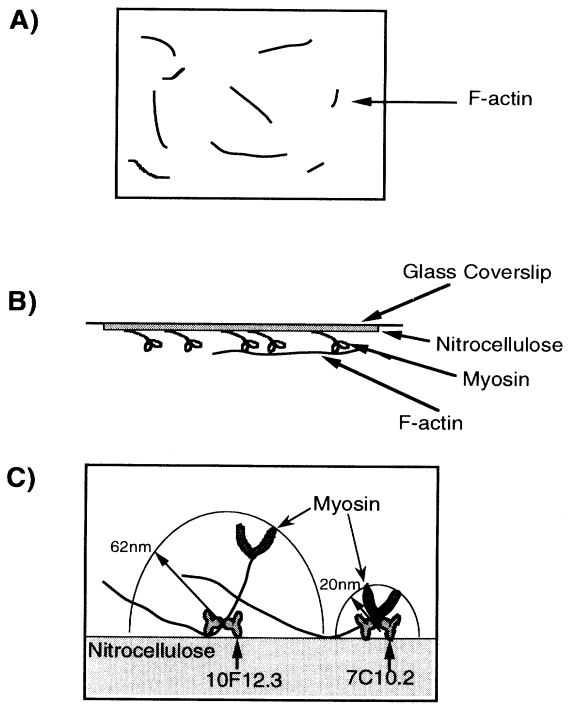

FIG. 1. Schematic diagrams of the *in vitro* experiment. (a) Top view of actin filaments on a myosin-coated coverslip, as obtained by fluorescence microscopy. (b) Cell cross section near the coverslip. (c) The ideal disposition of myosin tethered to the nitrocellulose surface by two different antibodies (7C10.2 and 10F12.3). The radius vector depicts the reaching distance from the attachment point to the actin binding surface on the myosin head.

*Author to whom correspondence should be addressed.

study the influence of temperature and motor surface density for fluorescent-labeled actin filaments sliding on myosin.

The study of velocity distributions implies a well-controlled preparation of the surfaces: myosin is tethered to a nitrocellulose surface by attachment to specific antibodies, according to a protocol described elsewhere [8]. Two different antibodies are used in order to vary the flexibility of the myosin attachment [Fig. 1(c)].

This study shows that the myosin attachment, the density of active motors, and the temperature are important parameters. In most cases, there is no velocity selection, but a broad distribution is observed covering velocities from zero to a finite value with a sharp exponential cutoff. The filament motion is dissipative, with successive stick and slip states.

In the case where a velocity is selected, a particular mode of attachment of myosin, a high motor surface density, and a high temperature are necessary. More specifically, an antibody binding within the myosin rod domain gives the best attachment of the myosin polymer to the nitrocellulose coated coverslip. The higher the myosin surface density, the better is the velocity defined. The temperature has to be close to the physiological temperature of the animal from which the proteins are extracted. Even in this case, defects of the flow appear. A defect is a pinning center for actin filaments. In this regime of high velocity, filaments anchored at a single point rotate around, defining a rotating spiral. Filaments anchored at more than one point cannot rotate. A flagellumlike motion develops. The radius of the rotating spiral gives a direct measure of the myosin driving force [9].

II. MATERIALS AND METHODS

A. Motility assays

Motility assays are performed according to a published protocol [8]. Myosin and actin are prepared from adult white leghorn chicken pectoralis muscle. For fluorescent labeling, actin is suspended overnight in the presence of phalloidin-rhodamine and then centrifuged to avoid background fluorescence. The labeled actin is diluted to 3 n*M* with a buffer which determines the *p*H, salinity, and MgATP concentration needed for optimal myosin motor activity [8] (25 m*M* Imidazole, 25 m*M* KCl, 7.5 m*M* $MgCl_2$, 0.2 m*M* $CaCl_2$, 5 m*M* 2-mercaptoethanol, 7.5 m*M* ATP, and *p*H 7.6). The buffer is supplemented with 0.5% 2-mercaptoethanol, 0.1 mg/ml glucose oxidase, 0.018 mg/ml catalase, and 2.3 mg/ml glucose to remove oxygen and with 0.5% methyl cellulose (1500 cP/2% aqueous solution) to confine the actin filaments close to the myosin surface.

Myosin is tethered to a nitrocellulose-coated coverslip by specific attachment to two different monoclonal antibodies [Fig. 1(c)]. One antibody, 7C10.2, reacts with a precise site near the myosin head (an epitope on the regulatory light chain LC2 located at the head-rod junction). The other, 10F12.3, reacts with a site in the rod domain (S2 region, 42 nm from the head-rod junction near the S2-LMM hinge). Myosin is first diluted to concentrations of 1 to 100 μg/ml in an high salt buffer [25 m*M* Imidazole (*p*H=7.6), 0.3*M* KCl, and 4 m*M* $MgCl_2$] supplemented with 1% bovine serum albumin. Antibody treated coverslips [8] are then incubated on 150 μl drops of the diluted myosin, leading to a specific attachment of myosin to the nitrocellulose-coated coverslip. The myosin surface density can be modified by varying the concentration of myosin in the solution. It is measured by radio-immunoassay with an accuracy of 10% [8].

The coated coverslips are mounted on 10 μl of labeled F-actin solution in the well of a Teflon-coated glass slide. A ring of vacuum grease is used to seal the sample. A typical sample thickness is 100 μm.

B. Optical microscopy

The motion of F-actin is observed by fluorescence microscopy using a Zeiss Axioscope equipped with a 63× Plan Apochromat objective, a 50 W mercury lamp, and a standard rhodamine filter set. Images are amplified using a 4× lens and projected onto an image intensifier (Hamamatsu Photonics) optically coupled to a Newvicon camera. For F-actin observation, fluorescence labeling is necessary because of the small actin cross section (8 nm). To avoid severe photo bleaching the light intensity must be reduced to a minimum value, and an image intensifier must be used.

C. Video analysis

Video segments are recorded on optical videodisk and then transferred to a Silicon Graphics workstation. Alternatively, images can be grabbed from a frame accurate VCR. The analysis proceeds in a number of steps. First, a single representative image is acquired so that the adjustable parameters of the filters can be set; readjustment is necessary since illumination, contrast, and background noise vary between experiments. The acquisition program uses these parameters and goes through every frame, performing the following calculations. A first program stores, thresholds, filters, creates a binary representation (filament–no filament), and finally compresses the database to give time, position, and shape of each filament. A second program gives an identity to each actin filament, and a third program defines the filament trajectory and the position of the filament on the track at each time. The precise operation is described in more detail below.

The first program performs the following operations:

(i) Grab the frame into memory [Fig. 2(a)]. Correct intensity and contrast with parabolic corrections.

(ii) Compute a histogram of pixel values to obtain an estimate of the typical background. A conservative estimate of a value X separating background from foreground is made. All pixel values are rescaled, so that the brightest pixel is mapped to 255 and all values below X are mapped to 0. This eliminates most of the background [Fig. 2(b)]; pixels that have a zero value are then ignored in future operations.

(iii) Apply a rank-depression filter [10]; every pixel is

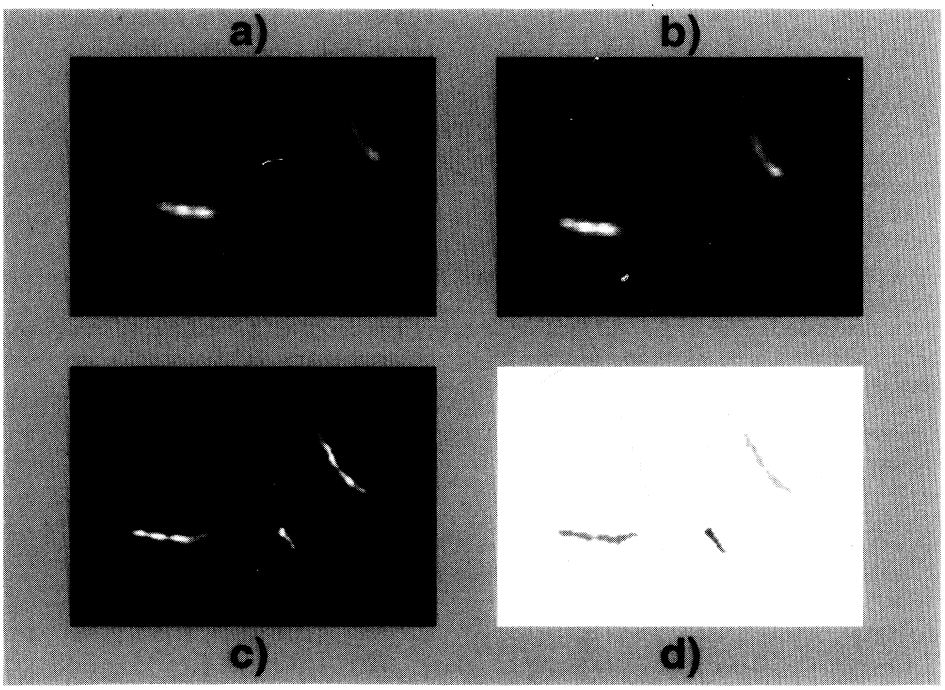

FIG. 2. Filtering of the video images. Each frame is filtered and acquired as explained in the text. (a) A video image (we show only a 15 μm$\times$12.5 μm section) (b) is thresholded, (c) refocused using the rank filter, and (d) finally digitized.

"ranked" against all pixels in a square matrix neighborhood. The value of each pixel is then multiplied by a monotone function of its own rank. The effect of this is to refocus the filaments [Fig. 2(c)]. The amount of refocusing is critical: if it is too small the filaments can be extremely thick; if it is too large, wavelength instabilities of the filter will develop, fragmenting the filament into pieces.

(iv) Threshold the image to a black and white binary representation; then separate all connected areas into distinct filaments [Fig. 2(d)] and save them in compressed format. At this point, a frame with about 20 filaments has been compressed to 4 Kbytes. We typically store 10 000 frames per dataset.

The second program reads these files and analyzes how every frame superimposes with the previous one, so that the continuity in time of the filaments can be established; a label can then be assigned to filaments, and this label can be propagated in time. Our current version cannot resolve ambiguities after two filaments have crossed each other, so both are assigned new labels. The lifetime of a given label is established, and in this case only the longest ones are kept in individual files. Thus, each of these files contains the shape of a single filament for a range of frames. Trajectories with fewer than 20 frames are discarded.

The third program reads the single-filament file. The shapes for all times are superimposed, and a skeleton of the resulting "track" is obtained (Fig. 3) and parametrized in arc length. Tracks shorter than 30 pixels are also discarded. For each frame, every pixel in the filament is projected onto this track; the minimum, maximum, and mean arc length coordinates are then computed. This is done so that, as a filament turns around a sharp corner, we obtain an unbiased estimate of the reptation speed of the filament. The output of this program is a file containing arc length positions along the track versus time (Fig. 4), which includes also the filament length. Thus concludes the data extraction stage; the data are now fully quantified.

III. EXPERIMENTAL RESULTS

A. Instantaneous velocities

Long trajectories are easily obtained. From ten minutes of videotape, about 100 tracks are usually resolved. Two skeletonized trajectories and successive positions of a filament at intervals of 2 s are shown in Fig. 3. In the upper panel, a filament (about 5 μm long) moves regularly and smoothly along the 140 μm long track, with an essentially constant velocity. In the lower one, a filament (about 4 μm long) stops twice in positions labeled 3 and 5. The mean arc length coordinate of this second filament is plotted as a function of time in Fig. 4(a). It shows that periods of motion with similar slopes (i.e., the same velocities) are separated by horizontal segments where the filament is in creeping motion, which correspond to positions 3 and 5 in Fig. 3 (lower panel). To measure instantaneous velocities on such a space-time curve, we divide it into segments. To find the optimum decomposition, the following iterative process is used. A straight line is traced, joining the beginning and the end of the space-time curve. The place of maximum distance of the experimental curve from the straight line defines the first break point. The process is iterated until the curve is well approximated. The termination of the seg-

mentation is chosen by the experimentalist. With each segment there is a corresponding velocity. Thus from each filament we obtain several velocities. The velocity is not projected onto an axis, but instead is measured along the trajectory. Histograms of the velocities are computed from the analysis of more than 100 filaments. To compute the distribution, each instantaneous velocity is weighted by its duration. The velocity interval (between the maximum and the minimum) is divided into 20 parts of equal length. The probabilities are normalized such that their sum is equal to 1. Let us recall that trajectories shorter than 30 pixels and 20 frames are discarded.

B. Distribution of instantaneous velocities

Let us analyze how the velocity distribution depends on the parameters of the system. Experiments are performed for the two different modes of myosin attachment (10F12.3 and 7C10.2) at MgATP concentration (7.5 mM), ionic strength (60 mM), and pH (7.6), parameters that optimize the velocity [8].

The velocity distribution obtained at five different temperatures between 10 and 30 °C, for the two antibodies, is shown in Fig. 5. For this study the myosin surface density, measured by radio-immunoassay, is close to saturation (900 molecules/μm^2).

Two different types of velocity distribution are observed:

(i) At low temperature for 10F12.3 (below 17.5 °C), and for almost all temperatures for 7C10.2, one observes a broad distribution with an exponential cutoff at high ve-

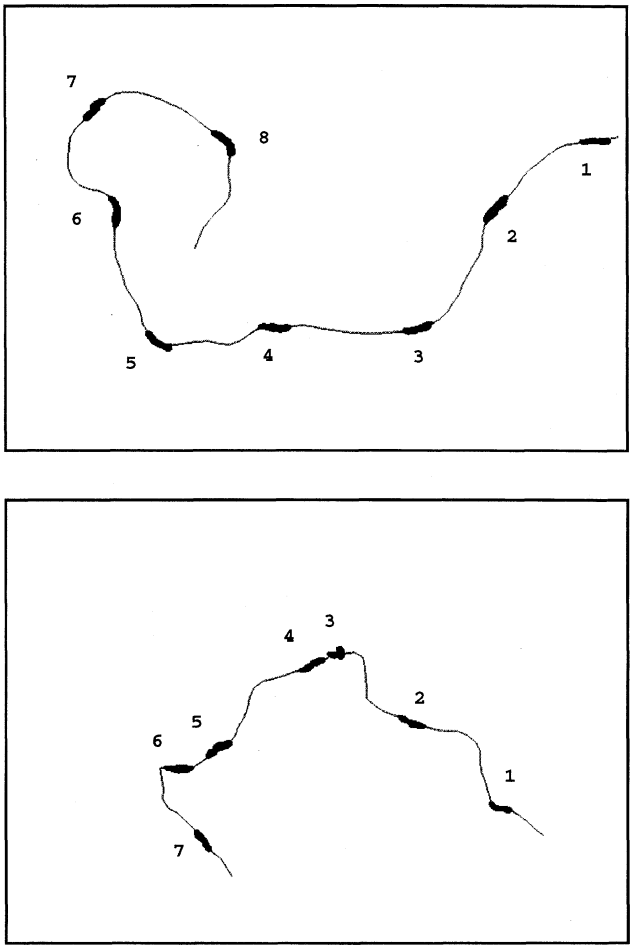

FIG. 3. Two filament trajectories. The images' size is 80 $\times$60 μm. Successive positions of the filaments on their tracks are indicated and labeled (time interval 2 s). The temperature is 32.5 °C, the myosin surface density is 900 molecules/μm^2, and the antibody is 10F12.3. In the upper panel, a filament moves smoothly without stopping on the 140 μm long track. In the lower panel, another filament from the same sample moves on a 100 μm track and stops twice in positions 3 and 5.

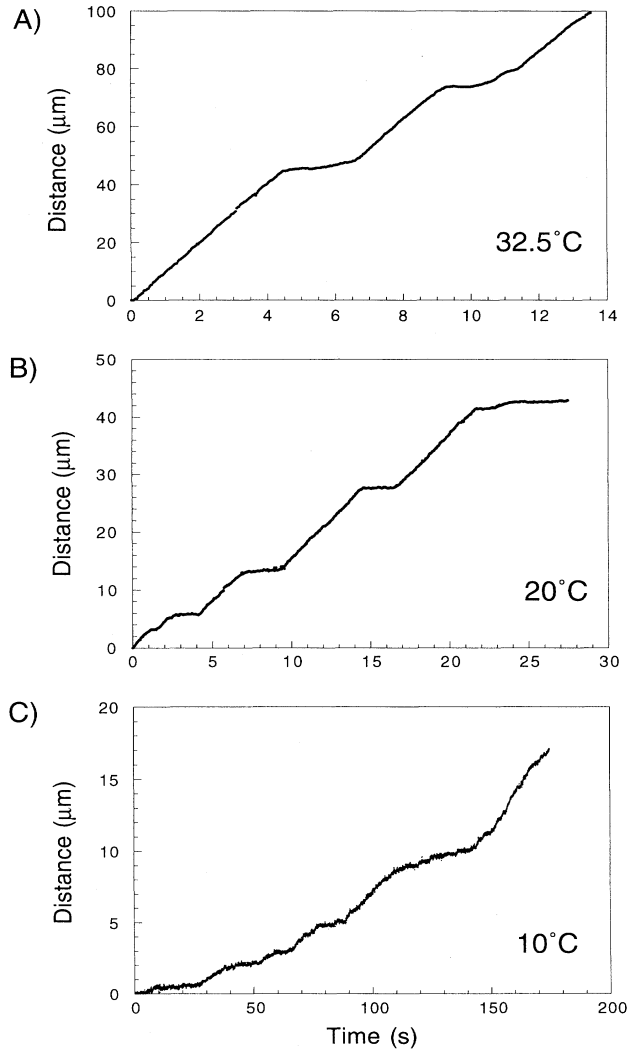

FIG. 4. Characteristic space-time curves (mean arc length coordinate vs. time) for three temperatures. The myosin surface density is 900 molecules/μm^2 and the antibody is 10F12.3. A space-time curve corresponds to the trajectory shown in Fig. 3 (lower panel). The pinning events shown in Fig. 3 and labeled 3 and 5 correspond to the plateau between 4.5 and 6.5 s and 9 and 10 s. Note that difference in scale among the three curves.

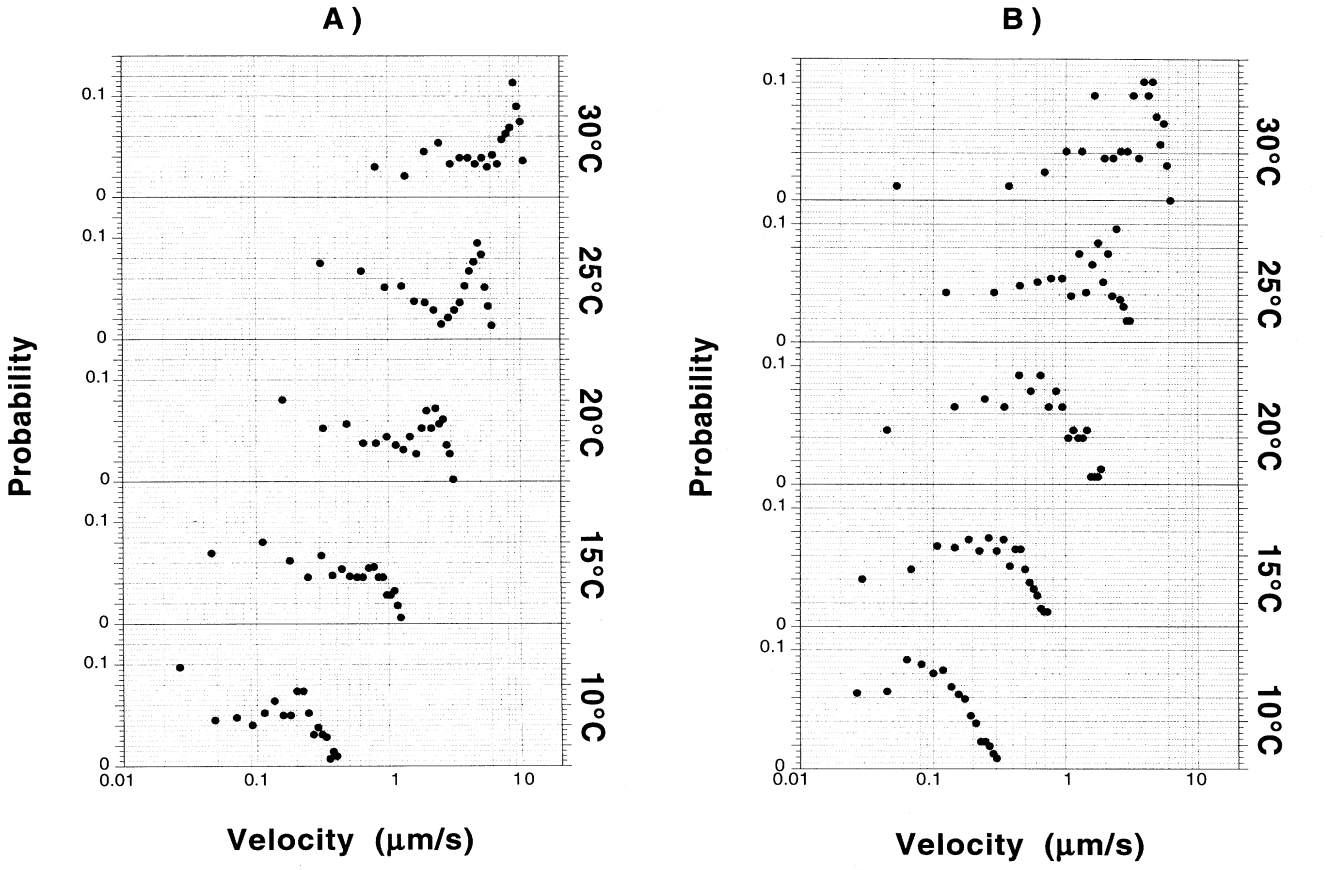

FIG. 5. Velocity distributions for (a) 10F12.3 and (b) 7C10.2, at 5 temperatures and at a myosin density of 900 molecules/μm^2. A logarithmic scale is used for velocity.

locity. In this low temperature regime there is no velocity selection and any velocity, up to the cutoff, is equally likely. One could of course define a mean value, but it is meaningless to talk about a velocity for F-actin.

(ii) On the contrary, at high temperatures (above 17.5 °C for 10F12.3, and at 30 °C for 7C10.2) the distribution is characterized by two peaks. One is near zero, the other at a finite and large value, and an exponential cutoff of the distribution is present at higher velocities. This implies a velocity selection and a regime of pinning where the filament is essentially fixed.

Clearly the mode of attachment of myosin within the rod domain (10F12.3) leads to higher velocities of F-actin, less friction, and a more effective kicking for the actin-myosin pair. It is a more flexible attachment, similar to the physiological attachment in the animal muscle.

The difference between the two distributions can be seen by comparing the space-time curves (Fig. 4). At high temperatures [Figs. 4(a) and (b), 10F12.3 antibody], long periods of regular motion (a few microns to several tens of microns) are seen, interrupted by states where the filament is essentially at rest. During the motion the velocity is well defined and constant. This leads to the two peaks in the velocity distribution. At low temperatures [Fig. 4(c), 10F12.3 antibody], several periods where the filaments are pinned are also observed. Between them, the velocity is undefined and changes constantly. This explains the broadband distribution seen in the histogram.

We have previously shown [8] that with 10F12.3 the "mean velocity" behaves differently below and above 17.5 °C. Similar breaks in the Arrhenius plot have been reported in other publications [6,11]. We now have an interpretation for this result: at high temperatures a well defined velocity exists; at low temperatures a regime of "stick-slip" is present. Let us recall [8] that, in the high temperature regime, the velocity increases rapidly with temperature [as $\exp(-E/T)$], with an apparent activation energy E close to 40 times the ambient temperature. This rapid increase in velocity is shown in Fig. 5(a).

Let us now consider how the velocity distribution depends on the myosin surface density. The surface density of motors can be controlled accurately by the specific attachment of myosin [8]. It can then be measured by radio-immunoassay, with 10% accuracy. This impressive control is one of the remarkable features of antibody based motility assays. Figure 6 shows the evolution of the instantaneous velocity distribution when the myosin

surface density varies from 900 to 25 molecules/μm^2, with a 10F12.3 antibody attachment, at a temperature of 25 °C.

A transition from a regime with a finite velocity to a regime with no preferential speed is also observed, as in the case of the temperature variation. This transition occurs at a surface density σ_{tr} of the order of 300 molecules/μm^2. A minimal kicking force on the filament is necessary to overcome friction and to define a clear velocity above the transition. But pinning is still present, leading to two distinct parts in the velocity distribution, one at low velocity, and the other one around 5 μm/s. Below the transition, the velocity distribution is broadband and decreases rapidly as the myosin surface density is reduced.

The peak velocity above σ_{tr} and the cutoff velocity below σ_{tr} are plotted in Fig. 7 as a function of the myosin surface density for a large number of samples. Above a characteristic density $\sigma_{sat} \sim 450$ molecules/μm^2, the velocity saturates; below this density, the velocity decreases linearly with decreasing σ.

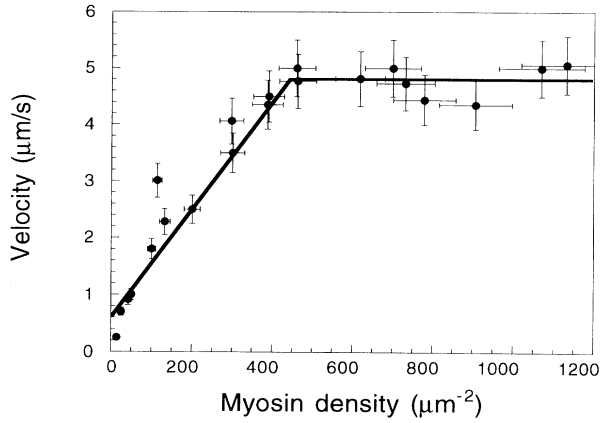

FIG. 7. F-actin velocity as a function of myosin surface density. A large number of data are used. The solid lines are guides for the eyes.

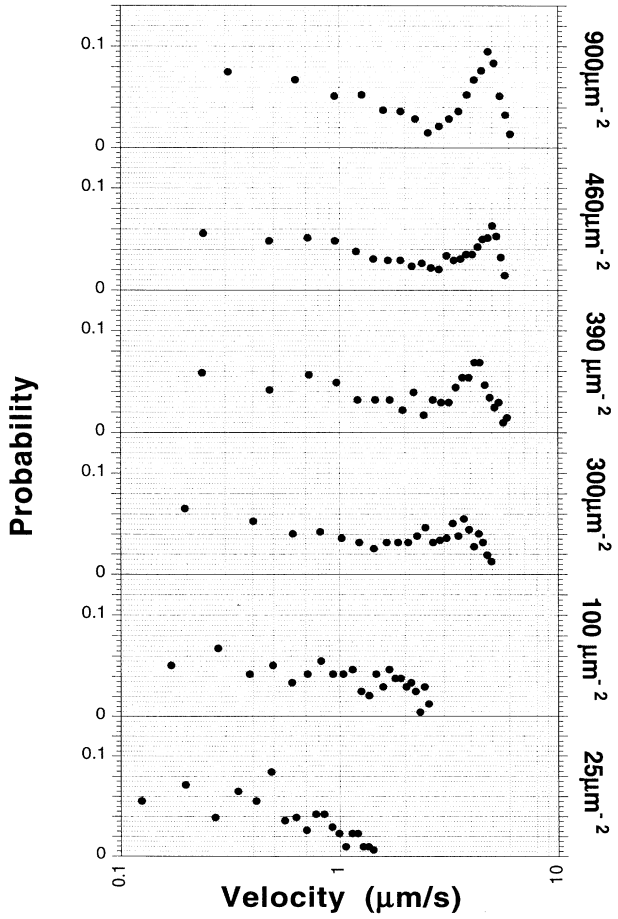

FIG. 6. Velocity distribution for 10F12.3, for six myosin surface densities; the temperature is 25 °C.

C. Defects in the flow: Rigid filaments, spirals, and flagella

Let us study the defects in the flow. At each temperature, filaments can be pinned for a finite time. There is no good model to describe pinning centers, but two possible explanations are a defective myosin head or a myosin vacancy. Pinning residence times are short, ten seconds at most, with a pinning potential of a few $k_B T$. The histogram of pinning times shows an exponential distribution with a mean value t_K, which is the mean escape time from the pinning potential and which is known as Kramers time. This time is temperature dependent, as shown in Fig. 8. It decreases with temperature as $\exp(E/T)$, the

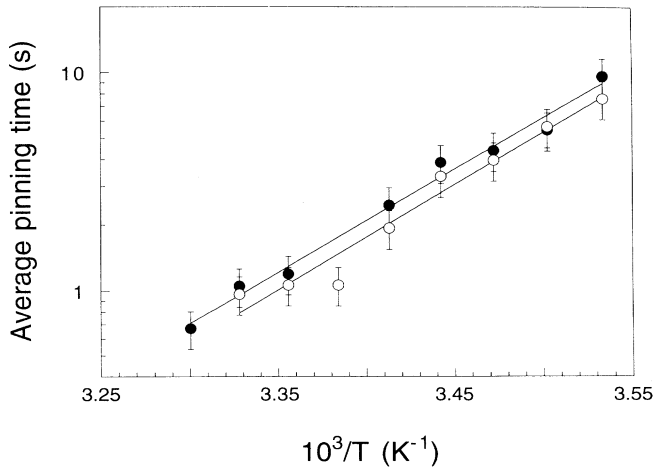

FIG. 8. Temperature dependence of the average pinning time for (●) 10F12.3 and (○) 7C10.2. The myosin density is 900 molecules/μm^2. The solid lines are fits of $\exp(E/k_B T)$ to the experimental points. E is $40 k_B T$ in both cases. Time is on a logarithmic scale.

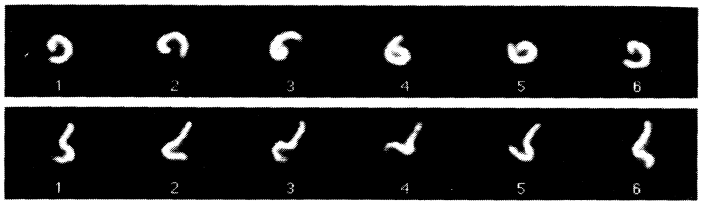

FIG. 9. Defects: (a) spiral, image size 9×54 μm; filament length 5 μm; (b) flagellum, image size 10×60 μm, filament length 6.5 μm. In both cases, the temperature is 27.5 °C, the myosin surface density is 900 molecules/μm^2, and the antibody is 10F12.3. The time interval between frames if 0.24 s.

apparent activation energy E being of the order to 40 times the ambient temperature, a behavior similar to the velocity. This is easy to understand; higher temperatures increase the actomyosin duty cycle and thus the mean kicking force, and Kramers escape time decreases.

Whereas residence times have a unique behavior, the pinning defects themselves depend on the F-actin length and the number of pinning points. All defects imply first the presence of a surface perturbation that fixes the leading edge of the actin filament. The myosin heads then apply a distributed force along the filament, in the direction of the leading edge. When the filament has a length such that it can buckle under this distributed force [9,12,13], it will rotate if the defect is pointlike and undulate like a flagellum if the defect has more than one pinning center. Both directions of rotation and undulation are observed to be equally likely. For a shorter free length the filament cannot buckle and will remain stationary until it escapes.

We call a rotating defect a spiral [Fig. 9(a)] and an undulating defect a flagellum [Fig. 9(b)]. If the pinning site is pointlike, the filament rotates around the fixed point as a spiral. If pinning extends over a segment, it cannot rotate any more but undulates like a flagellum. The mechanics and dynamics of these defects have been studied elsewhere [9]. An important point is that they are observed only in the regime where a well defined velocity exists. A more fundamental point, discussed in a preceding paper [9], is that the radius R of the rotating spiral gives a direct measure of the mean kicking force. If L_P is the F-actin persistence length and f the driving force per unit length, caused by the actin-myosin pairs, then the following scaling relation applies:

$$R \sim (k_B T L_P / f)^{1/3} .$$

Typically one measures a driving force of about 3 picoNewton, as R, L_P, and $k_B T$ are known [14,15].

IV. CONCLUSION

We have computed velocity distributions for a large number of actin filaments, using a computer program that extracts individual objects from a forest of moving filaments. Two different regimes of motion are identified. In the first regime a well defined flow velocity is observed with pinning sequences. Here, forces can be deduced from the study of spirallike defects [9]. The second regime does not show a unique flow velocity, but a broadband, up to a cutoff value. This regime appears at low temperatures or with a reduced myosin surface density. The mode of attachment of myosin to the substrate is important; attachment within the rod domain leads to a more flexible myosin head, and thus larger velocities.

The theoretical framework is difficult. One must take into account, at a microscopic level, driving forces, fluctuating friction, random pinning sites, and their temperature dependence. Currently the actin myosin cycle is only beginning to be understood [1,16]. Our only theoretical input has been, with collaborators, to introduce a scaling argument for defects [9].

ACKNOWLEDGMENTS

This work is supported by NSF Grant No. PHY-9408905. We thank T. Duke, L. Faucheux, and S. Leibler for their comments and advice.

[1] J. A. Spudich, Nature (London) **372**, 515 (1994); H. M. Warrick and J. A. Spudich, Annu. Rev. Cell Biol. **3**, 379 (1987).
[2] S. Leibler, Nature (London) **370**, 412 (1994).
[3] S. J. Kron and J. A. Spudich, Proc. Natl. Acad. Sci. (USA) **83**, 6272 (1986).
[4] Y. Harada, K. Sakurada, T. Aoki, D. D. Thomas, and T. Yanagida, J. Mol. Biol. **216**, 49 (1990).
[5] Y. Y. Toyoshima, S. J. Kron, and J. A. Spudich, Proc. Natl. Acad. Sci. (USA) **87**, 7130 (1990).
[6] E. Homsher, F. Wang, and J. R. Sellers, Am. J. Physiol. **262**, 714 (1992).
[7] D. E. Harris and D. M. Warshaw, J. Biol. Chem. **268**, 14 764 (1993).
[8] D. A. Winkelmann, L. Bourdieu, A. Ott, F. Kinose, and A. Libchaber, Biophys. J. **68**, 2444 (1995).
[9] L. Bourdieu, T. Duke, M. B. Elowitz, D. A. Winkelmann, S. Leibler, and A. Libchaber, Phys. Rev. Lett. **75**, 176 (1995).
[10] J. C. Russ, *The Image Processing Handbook* (CRC, Boca Raton, FL, 1992).
[11] M. P. Sheetz, R. Chasan, and J. A. Spudich, J. Cell Biol. **99**, 1867 (1984).
[12] L. D. Landau and E. M. Lifshitz, *Theory of Elasticity* (Pergamon, New York, 1986).
[13] F. Gittes, E. Meyhöfer, S. Baek, and J. Howard, Biophys. J. **66**, A312 (1994).
[14] A. Ott, M. O. Magnasco, A. J. Simon, and A. Libchaber, Phys. Rev. E **48**, R1642 (1993).
[15] J. T. Finer, R. M. Simmons, and J. A. Spudich, Nature (London) **368**, 113 (1994).
[16] C. Tesi, K. Kitagishi, F. Travers, and T. Barman, Biochemistry **30**, 4061 (1991).

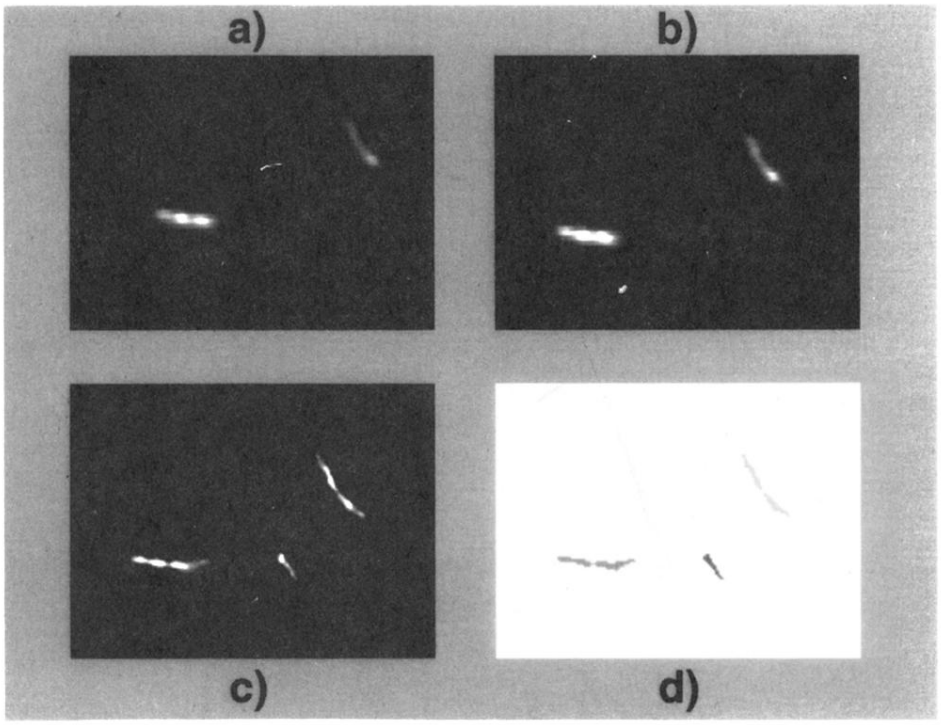

FIG. 2. Filtering of the video images. Each frame is filtered and acquired as explained in the text. (a) A video image (we show only a 15 μm$\times$12.5 μm section) (b) is thresholded, (c) refocused using the rank filter, and (d) finally digitized.

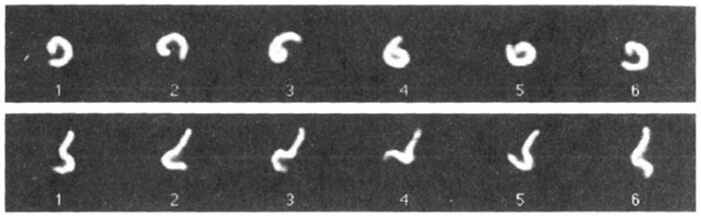

FIG. 9. Defects: (a) spiral, image size 9×54 μm; filament length 5 μm; (b) flagellum, image size 10×60 μm, filament length 6.5 μm. In both cases, the temperature is 27.5 °C, the myosin surface density is 900 molecules/μm^2, and the antibody is 10F12.3. The time interval between frames if 0.24 s.